Digital Communications and Networks 6 (2020) 14–22

Contents lists available at ScienceDirect

Digital Communications and Networks

journal homepage: www.keaipublishing.com/dcan

RFHUI: an RFID based human-unmanned aerial vehicle interaction system in an indoor environment*

Jian Zhang [a], Zhitao Yu [a,b], Xiangyu Wang [a,b], Yibo Lyu [a], Shiwen Mao [b,*], Senthilkumar CG. Periaswamy [a], Justin Patton [a], Xuyu Wang [c]

[a] Auburn University RFID Lab, Auburn, AL, 36849, USA
[b] Department of Electrical and Computer Engineering, Auburn University, Auburn, AL, 36849, USA
[c] Department of Computer Science, California State University, Sacramento, CA, 95819-6021, USA

ARTICLE INFO

Keywords:
Radio-Frequency Identification (RFID)
Human Computer Interaction (HCI)
Unmanned Aerial Vehicle (UAV)
Singular Value Decomposition (SVD)
Localization
Navigation

ABSTRACT

In this paper, we present an RFID based human and Unmanned Aerial Vehicle (UAV) Interaction system, termed RFHUI, to provide an intuitive and easy-to-operate method to navigate a UAV in an indoor environment. It relies on the passive Radio-Frequency IDentification (RFID) technology to precisely track the pose of a handheld controller, and then transfer the pose information to navigate the UAV. A prototype of the handheld controller is created by attaching three or more Ultra High Frequency (UHF) RFID tags to a board. A Commercial Off-The-Shelf (COTS) RFID reader with multiple antennas is deployed to collect the observations of the tags. First, the precise positions of all the tags can be obtained by our proposed method, which leverages a Bayesian filter and Channel State Information (CSI) phase measurements collected from the RFID reader. Second, we introduce a Singular Value Decomposition (SVD) based approach to obtain a 6-DoF (Degrees of Freedom) pose of the controller from estimated positions of the tags. Furthermore, the pose of the controller can be precisely tracked in a real-time manner, while the user moves the controller. Finally, control commands will be generated from the controller's pose and sent to the UAV for navigation. The performance of the RFHUI is evaluated by several experiments. The results show that it provides precise poses with 0.045 m mean error in position and 2.5° mean error in orientation for the controller, and enables the controller to precisely and intuitively navigate the UAV in an indoor environment.

1. Introduction

The application of Unmanned Aerial Vehicle (UAV), which originated in the military arena, has rapidly expanded to other areas, such as agriculture, research, commerce, and so on. Due to its prominent maneuverability, small form factor, and low cost, the UAV is widely adopted for surveillance, entertainment, search and rescue, and inspection for maintenance. In terms of personal UAV applications, over the past few years, more and more advanced algorithms and sensors have been introduced, which make their use increasingly powerful and comprehensive. These personal UAVs are usually used for human entertainment activities, such as taking photos and videos. The mounting growth of demands makes the interaction between the user and UAV a research topic attracting considerable interests [1].

In this paper, we propose RFID-based Human UAV Interaction (RFHUI), a low-cost, RFID-based system which provides an intuitive and easy-to-operate way to control and navigate a UAV in a complex indoor environment. The proposed method provides a means to precisely control a UAV to navigate it in a 3D space in a real-time manner. Specifically, we attach N ($N \geq 3$) Ultra High Frequency (UHF) passive RFID tags to a small board to create a hand-held controller. We record the position of each tag against the built-in coordinates of the controller. This position is denoted as a local one. We then deploy a Commercial Off-The-Shelf (COTS) RFID reader with multiple antennas to gather the observation

* This work was presented in part at EAI MobiQuitous2018, New York, NY, Nov. 6–8, 2018 [1].

* Corresponding author.
E-mail addresses: jzz0043@tigermail.auburn.edu (J. Zhang), zzy0021@tigermail.auburn.edu (Z. Yu), xzw0042@tigermail.auburn.edu (X. Wang), yzl0113@tigermail.auburn.edu (Y. Lyu), smao@auburn.edu (S. Mao), senthil@auburn.edu (S.CG. Periaswamy), jbp0033@auburn.edu (J. Patton), xuyu.wang@csus.edu (X. Wang).

https://doi.org/10.1016/j.dcan.2019.05.001
Received 28 October 2018; Received in revised form 6 March 2019; Accepted 7 May 2019
Available online 13 May 2019

of the tags. The global position, which refers to the global coordinates in the 3D space, of an RFID tag can be precisely tracked by the Channel State Information (CSI) phase measurements of the RFID tag responses from multiple antennas. A 6-DoF pose of the controller can be obtained from the known local position and estimated global position of the N attached tags. Finally, following the movement of the controller, the UAV responds and updates its pose and position in the air. The main contributions of this work can be summarized as follows:

1. A real-time RFID tag localizer is designed, which exploits the measured phase information of received RFID responses at a COTS reader. It localizes multiple UHF RFID tags simultaneously.
2. A real-time pose tracker is proposed. Based on the position of attached tags, a precise 6-DoF pose for the UAV controller is estimated in a 3D space.
3. We transform the pose of the controller into flying control commands for UAV navigation.
4. We implement the RFHUI system with COTS RFID devices and demonstrate its performance in a representative indoor environment. Experimental results show that the RFHUI can provide precise poses with 0.045 m mean error in position and 2.5° mean error in orientation for the controller. Thus, it enables the controller to precisely and intuitively navigate the UAV in an indoor environment.

The remainder of this paper is organized as follows. We review related works in Section 2. We present the design and analysis of the RFHUI system in Section 3 and our experimental study in Section 4. Section 5 concludes this paper.

2. Related works

With the development of robotics and growing demands for civilian and industrial applications, the concept of interaction and collaboration between human and robots has received a lot of attention. The study of Human Robot Interaction (HRI) focuses on how their communication achieves better real-time performance. It can be approximately divided into three areas of applications: teleoperation in specific environments [2–5], human-centric social interaction [6], and industrial manufacturing [7]. For applications in social interaction, Santos et al. proposed a tour-guide robot which is capable of recognizing the user's hand gesture and providing voice feedback [8]. In the field of HRI teleoperation in a specific environment, Urban Search And Rescue (USAR) is a very interesting research topic for deploying an HRI teleoperation in a specific environment. For example, Kohlbrecher et al. presented a human-robot system for rescue missions [9].

Compared to traditional robotic Unmanned Ground Vehicles (UGV), the UAV has significant differences, including flying freely, poor carrying capability, and being unsafe to touch. These demand a different and suitable new interaction method for human and UAV. The applications of Human Drone Interaction (HDI) are primarily focused on jogging companion UAVs involved in shooting videos, gesture recognition, and floating display. Muller et al. designed and built an outside jogging companion quadcopter system with GPS localization [10]. In Ref. [11], Scheible et al. proposed a system that combines a quadrocopter, a video projector, and a mobile phone for projecting contents onto walls or objects in an open space. Obviously, these UAVs are large and could only be used outdoors, thus prohibiting close interaction between human and drones. For gesture control applications, Cauchard et al. investigated the problem of multiple participants and found that natural gesture control leads to a more intimate relationship between user and UAV [12]. In the current commercial UAV market, DJI announced a state-of-the-art small gesture control based UAV product, called Spark [19], in May 2017. This is the first time that gesture recognition technologies have been introduced for consumer-class UAVs, enabling the removal of a traditional remote controller.

Since the last decade, RFID technology has been widely recognized as a promising solution for item serialization and tracking. Due to its cost-effective, lightweight, small form factor, and power-free properties, the RFID has also been widely deployed for indoor localization [20–27]. A considerable number of studies have focused on accessing the phase measurement of RF signals for localization [29,30]. Making use of Angle of Arrival (AOA) is a classic solution, which is driven by measuring the phase difference of the signals received at different antennas. In Ref. [30], Azzouzi presented the new measurement results for an AOA approach to localize RFID tags. In addition to localization applications, RFID technology has also been employed for 3-D reconstruction. Bu et al. proposed an approach based on the phase differences of RF signals for 3-D reconstruction of cubes [31], which is free of the limitation of line-of-sight and battery life constraint. Moreover, there are many other interesting scenarios that access RFID technology. For example, in Ref. [32], the reading patterns of RFID tags are leveraged to detect customers' behaviors in a physical clothes store. In Ref. [28], RFID tags are attached to the clothes of a patient to measure his/her respiration rate.

Motivated by the research of the aforementioned RFID applications, we go beyond the above HRI and HDI works to design a practical HDI navigation system based on the RFID technology and test it in a real-world laboratory environment. Compared to traditional vision-based HDI systems, the proposed RFHUI does not have the line-of-sight limitation due to the penetrating characteristics of RF signals.

3. RFHUI design and analysis

RFHUI is a low-cost, RFID-based system aiming to offer flexible human-UAV interaction. It provides an intuitive and easy-to-operate means for controlling a UAV in a 3D space. The RFHUI system comprises N ($N \geq 3$) UHF passive RFID tags and a COST RFID reader with M ($M \geq 2$) antennas. The tags are attached to the controller, and, when tracking the RFID tags by querying the phase information of each tag, a 6-DoF pose of the controller can be obtained. Then, the UAV can be controlled by this pose. In this section, we will introduce the system model and RFHUI architecture and design. Table 1 shows the important notations used in this paper.

Table 1
Important notations used in the paper.

Notation	Description
N	Amount of implemented RFID tags
M	Amount of RFID antennas
l_m	The position of the mth antenna in the global coordinate
x_t	The hypothetical posterior state of a dynamic system at a given time t. In RFHUI system, it refers to the position of an RFID tag at time t
u_t	The received control at time t. In RFHUI system, it denotes the speed of an RFID tag at time t
z_t	Observation at time t
$\mathscr{B}(x_t)$	The belief that denotes the probability of the system is in state x at time t. In RFHUI system, it refers to the probability of a tag in position x_t
$P(z_t \mid x_t, l_m)$	The observation model of the mth antenna
θ	RF phase measured from the reader
R	The distance between the reader antenna and an RFID tag
λ	Wavelength of the RF radio signal
$\theta_T, \theta_R, \theta_{TAG}$	The RF phase distortion caused by the reader's transmit circuits, the reader's receiver circuits, and the tag's reflection characteristics, respectively
$\widehat{X}_c, \widehat{Y}_c, \widehat{Z}_c$	Unit vectors of the axes of the built-in coordinates of the controller
$\widehat{X}_g, \widehat{Y}_g, \widehat{Z}_g$	Unit vectors of the axes in the global coordinates
$\boldsymbol{T}_t, \boldsymbol{R}_t$	The position and orientation of the controller at time t
$\boldsymbol{p}_n^t$	The position $(x_n^t, y_n^t, z_n^t)^T$ of the nth tag at time t in the global coordinates
${}_c^g\boldsymbol{T}_t$	The rigid transform between the controller's built-in coordinates and the global coordinates at time t
$\boldsymbol{H}_t$	Pose of the controller at time t
$\boldsymbol{U}_t$	Pose of the UAV at time t

3.1. System architecture

The system architecture of RFHUI is presented in Fig. 1. Our proposed RFHUI system consists of three main components as follows:

- *RFID Localizer*: We deploy a Bayesian filter to estimate the global location of the tags by utilizing the phase measurement from each tag, which is obtained by the reader.
- *Pose Tracker*: After the global location of N ($N \geq 3$) tags are obtained by the RFID localizer and combined with the given local location of each tag, we can track the pose of the controller with an SVD based method. Here, the local location is given in the built-in coordinate of the controller.
- *Control Module*: It converts the pose of the controller into flying control commands, which are transmitted to the UAV. Thus, the UAV can be navigated following a trajectory that is guided by the movement of the controller.

We present the design of the three components in the remainder of this section.

3.2. RFID localizer

In the RFHUI system, phase measurements of the tag responses are collected by an RFID reader with M antennas. We fix and measure the positions of all the antennas. Hereafter, let l_m denote the position of the mth antenna in the global coordinate.

3.2.1. Bayesian filter updates for tag localizing

In RFHUI, a Bayesian filter is deployed to localize the tags mounted on the controller. The Bayesian filter addresses the problem of estimating belief over the hypothetical posterior state x of a dynamic system by sensor observations. For the RFID localizer, the state x denotes the position of the tag against the global coordinate. The belief $\mathscr{B}(x_t)$, which denotes the probability that the system is in state x at time t, is recursively updated by the Bayesian filter. The update is calculated from control u_t, observation z_t, and prior belief $\mathscr{B}(x_{t-1})$ at time $(t-1)$, which is calculated previously.

Usually, one updating cycle of a typical Bayesian filter can be divided into two essential steps. Control update or prediction is the first step of the process, which is given as:

$$\overline{\mathscr{B}}(x_t) = \int P(x_t \mid u_t, x_{t-1}) \mathscr{B}(x_{t-1}) dx_{t-1} \tag{1}$$

where $P(x_t \mid u_t, x_{t-1})$ provides the probability of a tag moving from position x_{t-1} to x_t under the control of u_t, referred to as a motion model, and $\overline{\mathscr{B}}(x_t)$ represents the probability of the tag at position x_t after control u_t is executed. We assume that the speed of tags will remain constant for a very short time interval, and hence, a constant speed model can be deployed for the RFID localizer, which is expressed as:

$$P(x_t \mid u_t, x_{t-1}) = \frac{1}{\sqrt{2\pi}\delta} \int_0^{\Delta t} \exp\left\{ -\frac{(x_t - (x_{t-1} + u_t \cdot y))^2}{2\delta^2} \right\} dy \tag{2}$$

where u_t denotes the speed of the tag at time $t-1$ and Δt represents the time interval between $t-1$ and t.

Without loss of generality, we assume the movements of the tag satisfy a typical Gaussian distribution with standard deviation δ. The second step is the measurement update, which is written as:

$$\mathscr{B}(x_t) = \eta \cdot \overline{\mathscr{B}}(x_t) \cdot P(z_t \mid x_t) \tag{3}$$

In (3), η is a constant to integrate the sum of all $\mathscr{B}(x_t)$ into 1, and $P(z_t \mid x_t)$ represents the observation model. The RFID localizer is equipped with M reader antennas. Thus (3) can be rewritten as:

$$\mathscr{B}(x_t) = \sum_{m=1}^{M} \eta \cdot \overline{\mathscr{B}}(x_t) \cdot P(z_t \mid x_t, l_m) \tag{4}$$

where $P(z_t \mid x_t, l_m)$ denotes the observation model for the mth antenna. It provides the probability when the mth antenna in position l_m observes measurement z_t of the tag, which is in position x_t. The detail of the model is presented in the following.

3.2.2. Model of RFID phase measurement

The relationship of the RF phase shift between transmitted and received signals is given by the following equation:

$$\theta = \left(2\pi \cdot \left(\frac{2R}{\lambda} \right) + \theta_T + \theta_R + \theta_{TAG} \right) \bmod 2\pi \tag{5}$$

where θ is the RF phase measured by the reader, R is the distance between the reader antenna and the RFID tag, λ is the wavelength of the RF radio signal, $\theta_T, \theta_R, \theta_{TAG}$ are the RF phase distortion caused by the reader's transmit circuits, by the reader's receiver circuits, and by the tag's reflection characteristics, respectively, and mod is the Modulo operation.

Experiments show that for the same reader antenna, the same RFID tag, and the same radio frequency, θ_T, θ_R, and θ_{TAG} are fixed, and can be denoted as $\theta' = \theta_T + \theta_R + \theta_{TAG}$. Thus, (5) can be rewritten as:

$$\theta = \left(2\pi \cdot \left(\frac{2R}{\lambda} \right) + \theta' \right) \bmod 2\pi \tag{6}$$

We assume that a tag is in position x_{t-1} and a reader antenna in a position l_m observes the RF phase θ_1 from the tag's response. Under the same RF frequency, the tag moves to position x_t and the RF phase θ_2 is observed from the tag. The differential RF phase measurement between the two positions satisfies the following conditions:

$$\Delta\theta_{12} = (\theta_1 - \theta_2) \bmod 2\pi \tag{7}$$

$$\begin{aligned} \Delta\theta_{12} = &\left(\left(2\pi \left(\frac{2\left| x_{t-1} \cdot l_m^g \right|}{\lambda} \right) + \theta' \right) \bmod 2\pi \right. \\ &\left. - \left(2\pi \left(\frac{2\left| x_t \cdot l_m^g \right|}{\lambda} \right) + \theta' \right) \bmod 2\pi \right) \bmod 2\pi \end{aligned} \tag{8}$$

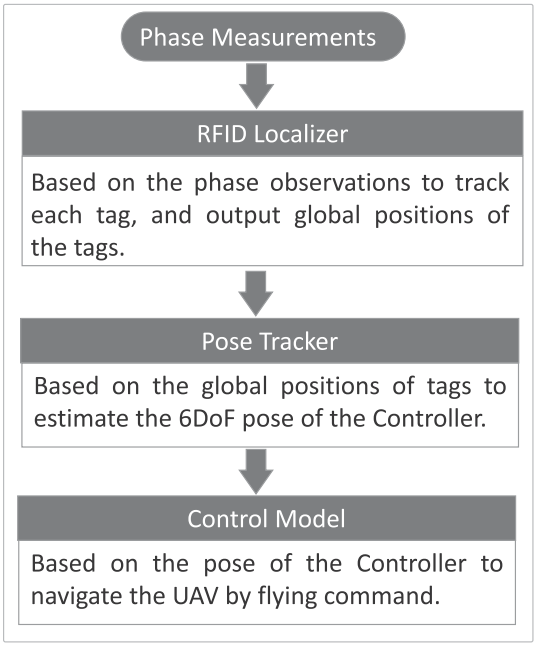

Fig. 1. The system architecture of RFHUI, where the global coordinates are built in the real world.

$$\Delta\theta_{12} = \left(\frac{4\pi}{\lambda}\cdot(|x_{t-1}\cdot l_m| - |x_t\cdot l_m|)\right) \bmod 2\pi \tag{9}$$

Equation (9) shows that under the same frequency for the same antenna and the same RFID tag, the differential RF phase $\Delta\theta_{12}$ is only determined by the distance the tag moves from x_{t-1} to x_t. In (9), $|x_t \cdot l_m|$ denotes the distance between the two positions. Hereafter, we assume that all the RF phases are measured for the same RFID reader and the same RFID tag under the same RF frequency. The tag moves in a discrete trajectory that is represented by a series of locations $x_1, x_2, \ldots, x_t$. The antenna, which is stationary in position l_m, collects the phase measurement for each location as $\theta_1, \theta_2, \ldots, \theta_m$. Then, the discrete trajectory of the movement of the tag should satisfy:

$$\begin{cases} \left|x_i\cdot l_m\right| - \left|x_j\cdot l_m\right| = \dfrac{\lambda}{4\pi}\cdot\Delta\theta_{ij} + n\cdot\dfrac{\lambda}{2} \\ \Delta\theta_{ij} = \left(\theta_i - \theta_j\right) \bmod 2\pi \\ n \in \{1,\ 2,\ 3,\ \ldots\} \\ i,j\,\varepsilon\{1,2,\ldots,t\} \text{ and } i \neq j \end{cases} \tag{10}$$

The observation model $P(z_t \mid x_t, l_m)$ can be updated by (10) to provide the probability that if a tag moves from x_{t-1} to x_t, the differential RF phase $\Delta\theta_{t,t-1}$ is obtained by the reader. We model the differential RF phase by the following equation:

$$P(\Delta\theta_{t,t-1} \mid x_{t-1}, x_t, l_m) = \begin{cases} 1, & \text{if (10) is satisfied} \\ 0, & \text{otherwise} \end{cases} \tag{11}$$

Let's consider the distortion of the RF phase that is caused by the thermal noise. Experiments reveal that the thermal noises introduces random errors to the phase measurement following a typical Gaussian distribution. Thus, we denote the RF phase as $\theta \sim \mathcal{N}(\mu,\delta)$, where μ is the RF phase without the distortion of thermal noise and δ denotes the standard deviation. Hence, we can update the differential RF phase as $\Delta\theta_{ij} \sim \mathcal{N}(\mu_i - \mu_j, \sqrt{2}\,\delta)$, and (11) can be updated as:

$$\begin{aligned} &P(\Delta\theta_{t,t-1} \mid x_{t-1}, x_t, l_m) \\ &= \frac{1}{\sqrt{2\pi}\delta}\int_0^{\Delta\theta_{t,t-1}} \exp\left\{-\frac{(y-(\mu_t-\mu_{t-1}))^2}{2\delta^2}\right\}dy \end{aligned} \tag{12}$$

$$\mu_t - \mu_{t-1} = \left(\frac{2|x_t\cdot l_m|}{\lambda} - \frac{2|x_{t-1}\cdot l_m|}{\lambda}\right) \bmod 2\pi \tag{13}$$

Based on (12), (13) and (4), we can estimate the locations of the RFID tags.

3.3. Pose tracker

The location of a tag, which is denoted as $\boldsymbol{p}_n^t = (x_n^t, y_n^t, z_n^t)^T$ for the nth tag at time t, can be estimated by the RFID localizer. When the controller is located at $\boldsymbol{T}$, with orientation $\boldsymbol{R}$ in the given global coordinate, $\boldsymbol{T}$ and $\boldsymbol{R}$ together are called the pose of the controller. Here, we denote the position of the controller at time t as $\boldsymbol{T}_t = (x_t, y_t, z_t)^T$, and the orientation at time t as

$$\boldsymbol{R}_t = \begin{bmatrix} \widehat{X}_c\cdot\widehat{X}_g & \widehat{Y}_c\cdot\widehat{X}_g & \widehat{Z}_c\cdot\widehat{X}_g \\ \widehat{X}_c\cdot\widehat{Y}_g & \widehat{Y}_c\cdot\widehat{Y}_g & \widehat{Z}_c\cdot\widehat{Y}_g \\ \widehat{X}_c\cdot\widehat{Z}_g & \widehat{Y}_c\cdot\widehat{Z}_g & \widehat{Z}_c\cdot\widehat{Z}_g \end{bmatrix} \tag{14}$$

where $\widehat{X}_c, \widehat{Y}_c$, and $\widehat{Z}_c$ represent the unit vectors of the axes of the built-in coordinates of the controller, and $\widehat{X}_g$, $\widehat{Y}_g$, and $\widehat{Z}_g$ denote the unit vectors of the axes in the global coordinates. The relationship of the two coordinates is illustrated in Fig. 2.

We measure the location of each attached tag in the controller's built-in coordinates, and the local location for the nth tag is denoted as $\overline{\boldsymbol{p}}_n = (\overline{x_n}, \overline{y_n}, \overline{z_n})^T$. The transformation between the global location and local location of the same tag is given by:

$$\begin{cases} \tilde{\boldsymbol{P}}_n^t = {}_c^g\boldsymbol{T}_t\cdot\overline{\boldsymbol{P}}_n \\ \tilde{\boldsymbol{P}}_n^t = \left(\boldsymbol{p}_n^t, 1\right)^T \\ \overline{\boldsymbol{P}}_n = \left(\overline{\boldsymbol{p}}_n, 1\right)^T \end{cases} \tag{15}$$

where ${}_c^g\boldsymbol{T}_t$ denotes the rigid transform at time t, $\boldsymbol{p}_n^t$ and $\overline{\boldsymbol{p}}_n$ is the location of the nth tag in the global coordinates and the controller's built-in coordinates, respectively. In (15), ${}_c^g\boldsymbol{T}_t$ comprises the pose of the controller in the global coordinate:

$${}_c^g\boldsymbol{T}_t = \begin{bmatrix} \boldsymbol{R}_t & \boldsymbol{T}_t \\ 000 & 1 \end{bmatrix} \tag{16}$$

where $\boldsymbol{R}_t$ and $\boldsymbol{T}_t$ denote the global orientation and global position of the controller at time t, respectively. Based on (15) and (16), we can obtain the pose of controller by searching an optimal transform ${}_c^g\boldsymbol{T}_t$. When the global locations of all the tags of the controller are provided by proposed RFID localizer, (15) can be updated as follows:

$$\begin{cases} \boldsymbol{p}_1^t = \boldsymbol{R}_t\cdot\overline{\boldsymbol{p}}_1 + \boldsymbol{T}_t \\ \boldsymbol{p}_2^t = \boldsymbol{R}_t\cdot\overline{\boldsymbol{p}}_2 + \boldsymbol{T}_t \\ \quad\ldots \\ \boldsymbol{p}_n^t = \boldsymbol{R}_t\cdot\overline{\boldsymbol{p}}_n + \boldsymbol{T}_t \end{cases} \tag{17}$$

where $\boldsymbol{p}_1^t$, $\boldsymbol{p}_2^t$, and $\boldsymbol{p}_n^t$ are the global locations for tag 1, 2, and n, respectively; and $\overline{\boldsymbol{p}}_1$, $\overline{\boldsymbol{p}}_2$, and $\overline{\boldsymbol{p}}_n$ are the local locations for tag 1, 2, and n, respectively. Therefore, the process of finding an optimal transform ${}_c^g\boldsymbol{T}_t$ can be formulated as a least square minimization problem as:

$$\min_{\{\boldsymbol{R}_t,\boldsymbol{T}_t\}} \sum_{i=1}^{N} \left\|\boldsymbol{p}_i^t - (\boldsymbol{R}_t\cdot\overline{\boldsymbol{p}}_i + \boldsymbol{T}_t)\right\| \tag{18}$$

where N is the total number of tags and $\|\cdot\|$ is the norm of a vector. Problem (18) is a typical problem of determining the rotation and translation relationship between two sets of data points at different coordinates, and a variety of methods have been introduced to solve such a problem [34,35]. Based on the approach that is introduced in Ref. [34], our proposed pose tracker is developed to find the optimal ${}_c^g\boldsymbol{T}_t$ in three steps:

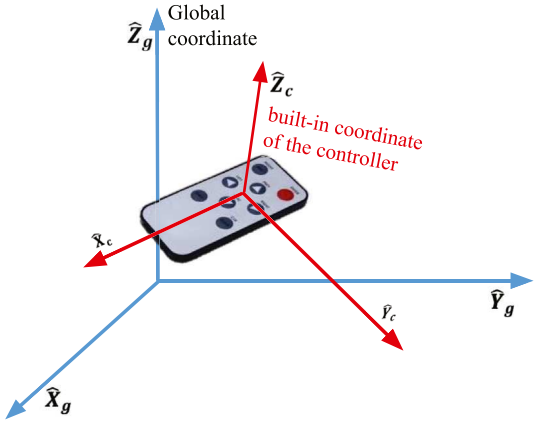

Fig. 2. The global coordinates versus the built-in coordinates of the controller.

Step 1. *Finding the centroids of all the locations in both global and local coordinates, which are denoted as* $\boldsymbol{C}$ *and* $\overline{\boldsymbol{C}}$*, respectively. Then, use the centroids as the new origins of two coordinates and transfer the locations into two coordinates, as:*

$$\begin{cases} \boldsymbol{p}_i^{t\prime} = \boldsymbol{p}_i^t - \boldsymbol{C}, & \text{for } i \in [1,2,\ldots,N] \\ \overline{\boldsymbol{p}}_i{}' = \overline{\boldsymbol{p}}_i - \overline{\boldsymbol{C}}, & \text{for } i \in [1,2,\ldots,N] \end{cases} \tag{19}$$

where N is the total number of tags.

Step 2. *Determining the optimal rotation* $\boldsymbol{R}_t$ *with the Singular Value Decomposition (SVD) method. First, cascade all the shifted locations of the tags in both global and local coordinates to form two matrices:*

$$\begin{cases} \boldsymbol{A} = [\boldsymbol{p}_1^{t\prime}{}', \boldsymbol{p}_2^{t\prime}{}', \ldots, \boldsymbol{p}_n^{t\prime}{}'] \\ \boldsymbol{B} = [\overline{\boldsymbol{p}}_1{}', \overline{\boldsymbol{p}}_2{}', \ldots, \overline{\boldsymbol{p}}_n{}'] \end{cases} \tag{20}$$

where both $\boldsymbol{A}$ *and* $\boldsymbol{B}$ *are* $3 \times N$ *matrices. Then, we decompose or factorize the matrix* $\boldsymbol{A}\boldsymbol{B}^T$ *with the SVD method as:*

$$[\boldsymbol{U}, \boldsymbol{D}, \boldsymbol{V}] = SVD(\boldsymbol{A}\boldsymbol{B}^T) \tag{21}$$

where $\boldsymbol{U}\boldsymbol{U}^T = \boldsymbol{V}\boldsymbol{V}^T = 1$*and* $\boldsymbol{D} = \mathrm{diag}(d_i), d_1 \geq d_2 \geq \cdots \geq d_n \geq 0$*. Based on the result in* Ref. [34]*, we obtain the optimal rotation* $\boldsymbol{R}_t$ *as:*

$$\boldsymbol{R}_t = \boldsymbol{U}\boldsymbol{S}\boldsymbol{V}^T \tag{22}$$

where

$$\boldsymbol{S} = \begin{cases} \boldsymbol{I}, & \text{if } \det(\boldsymbol{U})\det(\boldsymbol{V}) = 1 \\ \mathrm{diag}(1,1,\ldots,1,-1), & \text{if } \det(\boldsymbol{U})\det(\boldsymbol{V}) = -1 \end{cases} \tag{23}$$

In (23), $\mathbf{I}$ *is an identity matrix, and* $\mathrm{diag}(\cdot)$ *is a diagonal matrix.*

Step 3. *Obtaining the translation* $\boldsymbol{T}_t$*. After obtaining the rotation* $\boldsymbol{R}_t$*,* $\boldsymbol{T}_t$ *can be determined by the following equation:*

$$\boldsymbol{T}_t = \boldsymbol{C} - \boldsymbol{R}_t \cdot \overline{\boldsymbol{C}} \tag{24}$$

Therefore, based on the locations of the tags in both global and local coordinates, the proposed pose tracker can determine the controller's pose, including the orientation $\boldsymbol{R}_t$ and the position $\boldsymbol{T}_t$, referring to the global coordinates.

3.4. Human UAV interaction module

The human UAV interaction module primarily links the change of the controller's pose with UAV movement to achieve flexible remote control. We use the estimated pose of the controller to control the navigation of the UAV. To achieve real-time control, the UAV must react sensitively to the change of the controller's pose in a manner that follows the trajectory of the moving controller.

We use $\boldsymbol{H}_t$ to denote the pose of the controller, and $\boldsymbol{U}_t$ to denote the pose of the UAV at time *t*. The process of the module can be divided into four steps, which are detailed as follows:

1. Obtaining $\boldsymbol{H}_t$ and $\boldsymbol{H}_{t+1}$ from the pose tracker.
2. Calculating $\Delta\boldsymbol{H} = \boldsymbol{H}_{t+1} - \boldsymbol{H}_t$, which contains the change of position and orientation in the three-dimensional space.
3. Amplifying $\Delta\boldsymbol{H}$ as $\Delta\boldsymbol{H}' = \alpha \cdot \Delta\boldsymbol{H}$, where α is the parameter of the amplification, and we usually set $\alpha = 5$. We can make a slight movement of the controller to activate a large-scale movement of the UAV.
4. Converting the $\Delta\boldsymbol{H}'$ to flying control commands and send it to the UAV.

Step 4 cooperates with the specific UAV platform, and it usually relies on the API to communicate with the UAV. For example, in our experimental platform, an ROS [33] based system is developed to communicate with the ARDrone2.0 platform [13]. It updates the target position of the UAV by

$$\boldsymbol{U}_{t+1} = \boldsymbol{U}_t + \Delta\boldsymbol{H}' \tag{25}$$

and sends the $\boldsymbol{U}_{t+1}$ to the UAV through the ROS message service.

4. Experimental validation and results

4.1. Experiment setup

We conduct a series of experiments to demonstrate the performance of the RFHUI system. We establish a prototype of RFHUI using a COTS reader and several UHF passive RFID tags. A Zebra FX7500 RFID reader [14] with four Zebra AN720 antennas [15] is incorporated to query the RFID tags. The Zebra FX7500 reader is widely deployed in retail, manufacture factory, and warehouse applications, and meets the EPC Gen2 standard requirements [16].

In our prototype system, we use the Low-Level Reader Protocol (LLRP) through an Ethernet port to communicate with the reader and report the RFID measurements. The Zebra AN720 Antennas provide a left circular polarization with a 100° beam width and a 5.5 ∼ 6 dB gain. Each antenna is mounted on a holder of 1.4 m height. The four antennas with their holders are deployed in front of the user. In all our experiments, we set the reader to work at the maximum RF transmission power, i.e., 33 dBm, to enable each antenna to gain a detectable range up to 6 m. Our experimental setting is illustrated in Fig. 3 (side view) and Fig. 4 (top view). The configuration of the four antennas created a detectable field, which allows the four antennas to interrogate an RFID tag simultaneously.

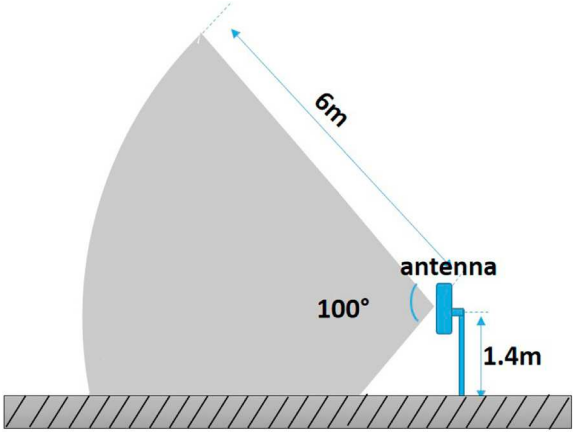

Fig. 3. Side view of the RFID detectable field.

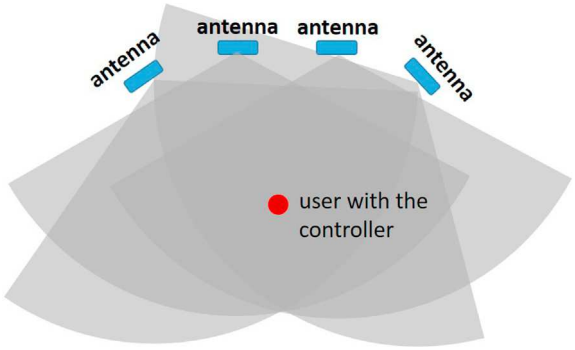

Fig. 4. Top view of the RFID detectable field.

Three UHF passive RFID tags are attached to a foam board working as our prototype controller, which is shown in Fig. 5. Fig. 6 shows how the controller is operated by a user during the tests. Our experimental RFID tag is Smartrac Dogbone Monza R6 [17], which is widely used in the retail business. We choose the Parrot ARDrone2.0 Elite Edition drone [18] as our UAV platform, which is shown in Fig. 7. It is equipped with a front camera, a bottom camera, a sonar, and an Inertial Measurement Unit (IMU). Based on the measurements of the onboard sensors, it can localize itself by using a sensor fusion method. For example, the Parallel Tracking and Mapping (PTAM) technique [19] can be implemented to estimate the 3D pose of the ARDrone2.0 drone.

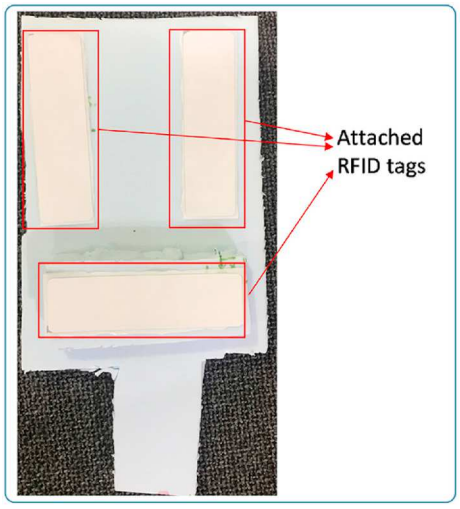

Fig. 5. A prototype of our RFHUI controller.

Fig. 6. A user holds the controller in hand during an experiment.

Fig. 7. The ARDrone2.0 Elite Edition drone used in our experiments.

4.2. Accuracy of RFID tracking and pose estimation

4.2.1. Effect of the number of antennas

Before revealing the performance of the proposed RFHUI system, we first conduct a set of benchmark experiments to discover the effect of the number of RFID antennas on the system performance. We configure the RFID reader with 1, 2, 3, and 4 antennas in each benchmark experiment, respectively. During every benchmark experimentation, the controller is moved along the same trajectory, which is shown in Fig. 8. We first moved the controller with 20 cm in the direction of the x-axis, and then moved it for another 20 cm along the y-axis direction. We sampled the trajectory every 2 cm, which is illustrated by the red points in Fig. 8. There were totally 21 sampled points. At every sampled point we record the ground truth location and the estimated location that are provided by the RFID localizer for every tag and collect the ground truth and the estimated pose of the controller.

First, we evaluate the accuracy of the RFID localizer by comparing the estimated location to the ground truth location of every tag at all sampled points. The average location error of each tag at different antenna configurations is shown in Fig. 9. We can see that the more antennas are deployed, the more accurate the estimated localization. The results are consistent with the conclusion of (4): the more antennas are deployed, the more accurate estimation can be made.

We also evaluate the accuracy of the controller's pose, including position and orientation, which is measured by our RFHUI system. The results in each antenna configuration are shown in Fig. 10 and Fig. 11. From Figs. 10 and 11, the average errors of both position and orientation

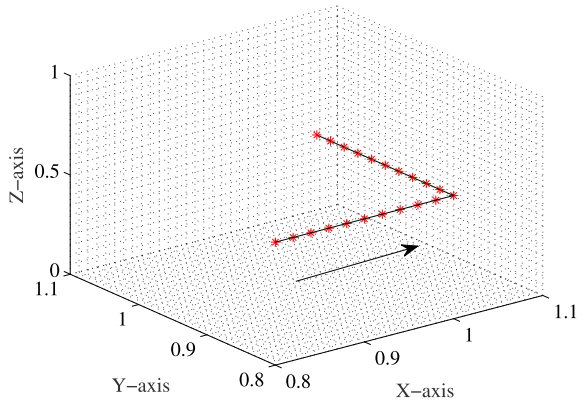

Fig. 8. The moving trajectory of the benchmark experiments: the red points are the sampled locations.

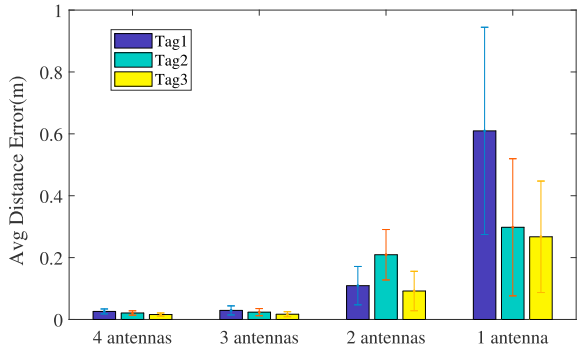

Fig. 9. The average error and standard deviation of the localization error of the controller's tags for different antenna configurations.

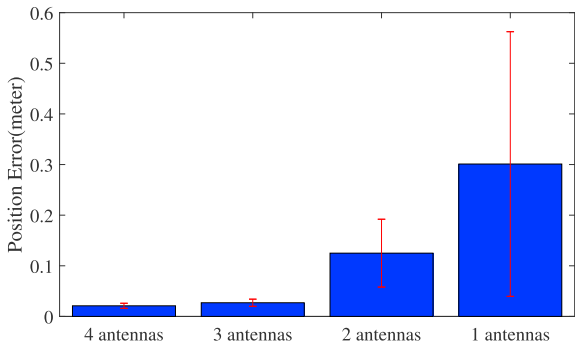

Fig. 10. The average position error of the controller for different antenna configurations.

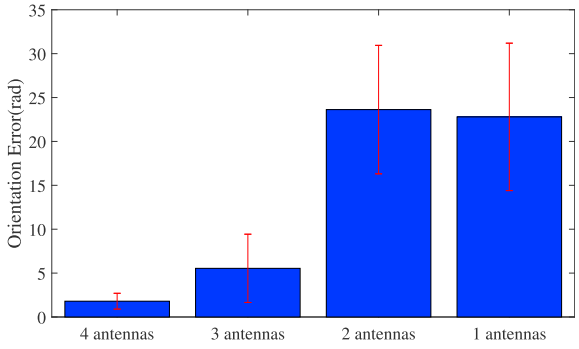

Fig. 11. The average orientation error of the controller for different antenna configurations.

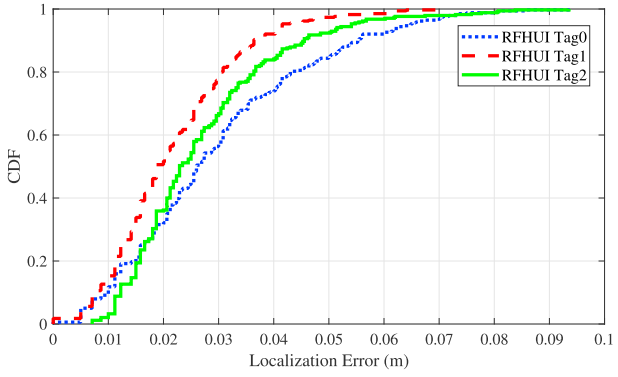

Fig. 12. CDF of RFID tags tracking error with a more complex and longer trajectory.

are reduced dramatically when the number of deployed antennas is increased. For the configuration with 4 antennas, the system achieves an average error of 0.021 m in position and 1.8˚ in orientation. Therefore, all hereafter experiments are implemented with the 4-antenna configuration with the setup shown in Fig. 4.

4.2.2. *RFID tags tracking*

To evaluate the performance of the RFID localizer in RFHUI, we launch another experiment by attaching three UHF passive RFID tags to the controller. A user holds the controller and moves it following a given trajectory, which is inside the experiment field. In contrast to the simple trajectory in our benchmark experiments, we move the controller in a more complex and longer trajectory with more variety in moving direction, thus to mimic the actual user behavior while operating the UAV. During the experiment, the RFID localizer of RFHUI provides estimated

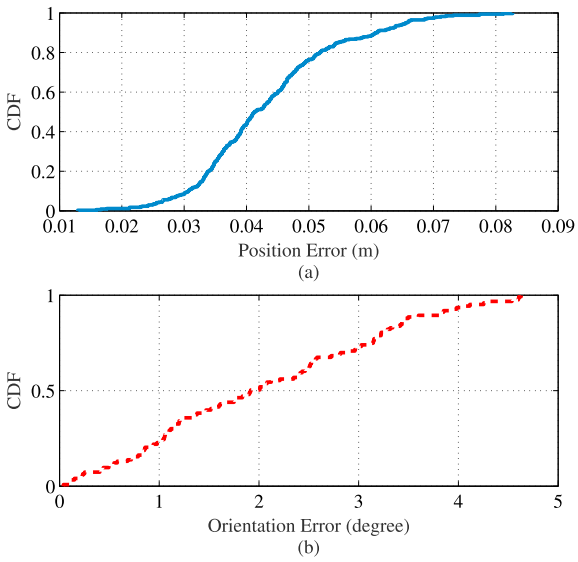

Fig. 13. (a) CDF of the controller position estimation error; (b) CDF of the controller orientation error.

locations for each tag while the controller is moving. We obtain the ground-truth locations by measuring the sampled points every 5 mm along the trajectory. The accuracy of the proposed method is evaluated by calculating the errors between the ground-truth locations and the estimated locations of the sampled points.

We repeat the experiment several times, and the experimental results are presented in Fig. 12 in the form of the Cumulative Distribution Function (CDF) of localization errors between estimated and ground-truth positions. We can see that the maximum error of the RFID localizer is less than 0.095 m for all the three tags. Moreover, with the RFID localizer of RFHUI, 80% of the localization errors are less than 0.045 m and 90% of them are under 0.06 m. Therefore, it is safe to state that the RFID localizer achieves very precise localization for tracking the moving RFID tags. Note that the average error of every tag is a little bit higher than that in the benchmark experiments because we consider much more sampled points and the controller moves along a more complex trajectory in this experiment.

4.2.3. *Controller pose estimation*

We next conduct an experiment to verify the feasibility and accuracy of our proposed pose tracker, including position and orientation estimations. The controller moves along a trajectory in our experiment field, held by a user.

The results are presented in Fig. 13. Fig. 13(a) shows that about 78% of the position errors of the proposed pose tracker are under 0.05 m, and the maximum error is less than 0.083 m. Additionally, as shown in Fig. 13(b), we can see that 60% the orientation errors are less than 2.5˚. Moreover, for the pose tracker, almost 90% of the orientation estimations achieve an error under 3.5˚. Obviously, regardless of position and orientation estimations, the proposed pose tracker of RFHUI is sufficiently accurate for most practical human-UAV interaction scenarios. Also note that similar to the result in the of RFID tags tracking experiment, due to the greater number of sampled points and increased complexity of the moving trajectory in this experiment, the average of errors in both position and orientation is a little bit higher than that in the benchmark experiments.

4.3. *Overall system performance*

Finally, we conducted an experiment in our indoor lab environment to demonstrate the feasibility of our system in a real-time manner. The typical experimental environments are shown in Fig. 14 and Fig. 15. The

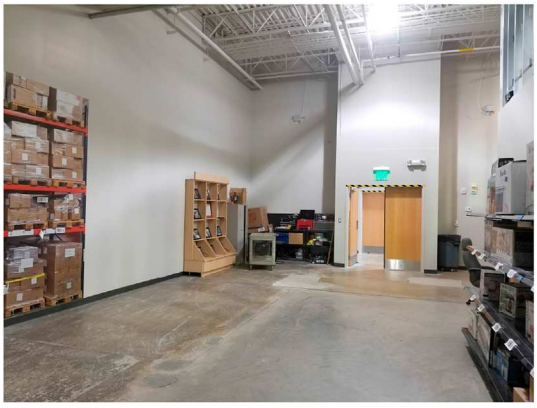

Fig. 14. The empty lab environment.

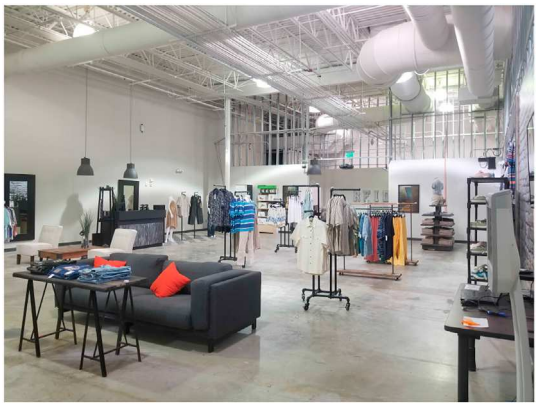

Fig. 15. The cluttered lab environment.

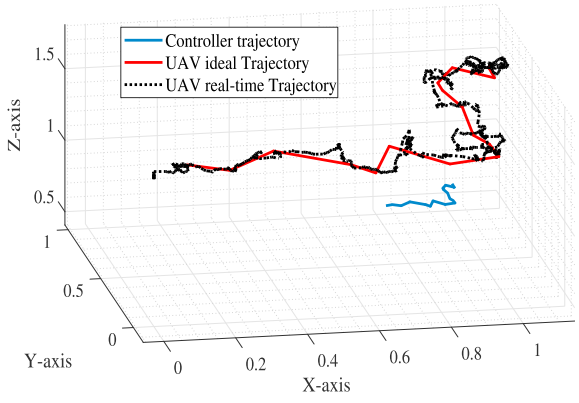

Fig. 16. Trajectory comparison.

complex indoor environment, with intricate features and layouts with shelves, clothes stands, and furniture as shown in Fig. 15, requires our proposed RFHUI system to provide an accurate and robust control method to safely operate the UAV indoors. During this experiment, a user holds the controller, which is attached with 3 RFID tags, to control the UAV. We compared the ideal movement trajectory of the UAV, which is amplified by the trajectory of the controller, and the actual movement of the UAV to illustrate the performance of the proposed RFHUI.

A typical experiment result is presented in Fig. 16. The movement of the controller follows a random trajectory, which is illustrated by the black curve in Fig. 16. The blue curve represents the trajectory of the controller. The red curve denotes the ideal trajectory of the UAV, which is an amplified version of the trajectory of the controller. Clearly, we can tell that the UAV precisely follows the ideal trajectory, with only tiny disturbances around the ideal occurred. This is caused by the inherent errors of the UAV, especially when the UAV is in a hovering mode. It is apparent that our RFHUI system achieves high accuracy in real-time navigation. This experiment validates that our RFID-based controller strategy is robust and practical. This is mainly due to the fact that our proposed RFHUI system can provide a highly accurate pose estimation, which plays a critical role in UAV navigation.

5. Conclusions

In this paper, we proposed the RFHUI, an RFID based system for navigation control of a UAV using a COTS RFID reader. We experimentally validated the feasibility of utilizing an RFID localization-based method as the core of the UAV controller. We leveraged a Bayesian filter to estimate the location of RFID tags using the phase information in RFID tag responses. Then an SVD algorithm was employed for data preprocessing to track the pose of the controller. Finally, the control module converted the pose data into flying control commands to achieve UAV navigation control in real-time. The extensive experiments in a representative lab environment demonstrated the capability of the proposed RFHUI system. To the best of our knowledge, the proposed RFHUI is the first practicable UHF passive RFID based UAV navigation control system, which provides a promising method for Human-UAV interaction.

Acknowledgements

This work is supported in part by the US NSF under Grant CNS-1702957 and ECCS-1923163, and by the Wireless Engineering Research and Education Center (WEREC) at Auburn University.

References

[1] J. Zhang, Z. Yu, X. Wang, Y. Lyu, S. Mao, S.C.G. Periaswamy, J. Patton, X. Wang, RFHUI: an intuitive and easy-to-operate human-UAV interaction system for controlling a UAV in a 3D space, in: Proc. EAI MobiQuitous 2018, New York City, NY, Nov, 2018, pp. 69–76.
[2] J.L. Casper, R.R. Murphy, "Workflow study on human-robot interaction in USAR," in Proc, in: 2002 IEEE International Conference on Robotics and Automation, Washington, DC, May 2002, pp. 1997–2003.
[3] H. Jones, S. Rock, D. Burns, S. Morris, Autonomous robots in swat applications: research, design, and operations challenges, in: Proc. 2002 Symposium for the Association of Unmanned Vehicle Systems International, AUVSI '02), Orlando, FL, July 2002, pp. 1–15.
[4] M. Li, K. Lu, H. Zhu, M. Chen, S. Mao, B. Prabhakaran, Robot swarm communication networks: architectures, protocols, and applications, in: Proc. Chinacom'08, Hangzhou, P.R. China, Aug. 2008, pp. 162–166.
[5] M. Li, J. Harris, M. Chen, S. Mao, Y. Xiao, W. Read, B. Prabhakaran, Architecture and protocol design for a pervasive robot swarm communication networks, Wiley Wirel. Commun. Mob. Comput. J. (WCMC) 11 (8) (Aug. 2011) 1092–1106.
[6] C. Bartneck, J. Forlizzi, A design-centered framework for social human-robot interaction, in: Proc. International Workshop on Robot and Human Interactive Communication, Kurashiki, Japan, Sept. 2004, pp. 591–594.
[7] O.O. Ogorodnikova, Safe and reliable human-robot interaction in manufactory, within and beyond the workcell, in: Proc. 19th International Workshop on Robotics in Alpe-Adria-Danube Region, Budapest, Hungary, June 2010, pp. 65–70.
[8] V. Alvarez-Santos, R. Iglesias, X.M. Pardo, C.V. Regueiro, A. Canedo-Rodriguez, Gesture-based interaction with voice feedback for a tour-guide robot, J. Vis. Commun. Image Represent. 25 (2) (Feb. 2014) 499–509.
[9] S. Kohlbrecher, A. Romay, A. Stumpf, A. Gupta, O. von Stryk, F. Bacim, D.A. Bowman, A. Goins, R. Balasubramanian, D.C. Conner, "Human-robot teaming for rescue missions: team ViGIR's approach to the 2013 DARPA Robotics Challenge trials, J. Field Robot. 32 (3) (May 2015) 245–267.
[10] F. Mueller, M. Muirhead, Jogging with a quadcopter, in: Proc. 33rd Annual ACM Conference on Human Factors in Computing Systems, Seoul, Republic of Korea, Apr. 2015, pp. 2023–2032.
[11] J. Scheible, A. Hoth, J. Saal, H. Su, Displaydrone: a flying robot based interactive display,, in: Proc. 2nd ACM International Symposium on Pervasive Displays, Mountain View, CA, June 2013, pp. 49–54.
[12] J.R. Cauchard, J.L.E. Kevin, Y. Zhai, J.A. Landay, Drone & me: an exploration into natural human-drone interaction, in: Proc. UbiComp'15, Osaka, Japan, Sept. 2015, pp. 361–365.
[13] Parrot ARDrone2.0 [online] Available: https://www.parrot.com/global/drones/parrot-ardrone-20-elite-edition#parrot-ardrone-20-elite-edition. Accessed on June. 4, 2018.

[14] Zebra, Fx7500 [online] Available: https://www.zebra.com/us/en/products/rfid/rfid-readers/fx7500.html. Access on June. 4, 2018.
[15] Zebra, An720 [online] Available: https://www.zebra.com/us/en/products/rfid/rfid-reader-antennas/an720.html. Accessed on June. 4, 2018.
[16] GS1 US [online] Available: https://www.gs1us.org/. Accessed on June. 4, 2018.
[17] Samrtarc, Dogbone, Accessed on June. 4, 2018, http://www.smartrac%5c-group.com/files/content/_Products%5c-Services/PDF/0028%5c_SMARTRAC%5c_DOGBONE.pdf.
[18] G. Klein, D. Murray, Parallel tracking and mapping for small AR workspaces, in: Proc. 6th IEEE and ACM International Symposium on Mixed and Augmented Reality, Nara, Japan, Nov. 2007, pp. 225–234.
[19] DJI, SPARK [online] Available: https://www.dji.com/spark. Accessed on June. 4, 2018.
[20] F. Gandino, B. Montrucchio, M. Rebaudengo, E.R. Sanchez, On improving automation by integrating RFID in the traceability management of the agri-food sector, IEEE Trans. Ind. Electron. 56 (7) (July 2009) 2357–2365.
[21] L. Jing, P. Yang, A localization algorithm for mobile robots in RFID system, in: Proc. 2007 International Conference on Wireless Communications, Networking and Mobile Computing, Wuhan, China, Sept. 2007, pp. 2109–2112.
[22] P. Yang, W. Wu, M. Moniri, C.C. Chibelushi, SLAM algorithm for 2D object trajectory tracking based on RFID passive tags, in: Proc. IEEE RFID 2008, Las Vegas, NV, Apr. 2008, pp. 165–172.
[23] A. Bekkali, H. Sanson, M. Matsumoto, RFID indoor positioning based on probabilistic RFID map and Kalman Filtering, in: Proc. Third IEEE International Conference on Wireless and Mobile Computing, Networking and Communications, White Plains, NY, Oct. 2007, p. 21.
[24] P.V. Nikitin, R. Martinez, S. Ramamurthy, H. Leland, G. Spiess, K.V.S. Rao, Phase based spatial identification of UHF RFID tags, in: Proc. IEEE RFID'10, Orlando, FL, Apr. 2010, pp. 102–109.
[25] J. Zhang, Y. Lyu, J. Patton, S. Chinnappa Gounder P, T. Roppel, BFVP: a probabilistic UHF RFID tag localization algorithm using Bayesian filter and a variable power RFID model, IEEE Trans. Ind. Electron. 65 (10) (Oct. 2018) 8250–8259.
[26] T.M. Choi, Coordination and risk analysis of VMI supply chains with RFID technology, IEEE Trans. Ind. Informat. 7 (3) (Aug. 2011) 497–504.
[27] X. Wang, C. Yang, S. Mao, SparseTag: High-precision backscatter indoor localization using sparse RFID tags array, in: Proc. IEEE SECON 2019, Boston, MA, June 2019, pp. 1–9.
[28] C. Yang, X. Wang, S. Mao, AutoTag: Recurrent vibrational autoencoder for unsupervised apnea detection with RFID tags, in: Proc. IEEE GLOBECOM 2018, Abu Dhabi, United Arab Emirates, Dec. 2018, pp. 1–6.
[29] Y. Zou, Survivable RFID systems: issues, challenges, and techniques, IEEE Trans. Syst. Man Cybern. C (Appl. Rev.) 40 (4) (July 2010) 406–418.
[30] S. Azzouzi, M. Cremer, U. Dettmar, R. Kronberger, T. Knie, New measurement results for the localization of UHF RFID transponders using an Angle of Arrival (AoA) approach, in: Proc. IEEE RFID'11, Orlando, CA, Apr. 2011, pp. 91–97.
[31] Y. Bu, L. Xie, J. Liu, B. He, Y. Gong, S. Lu, 3-dimensional reconstruction on tagged packages via RFID systems, in: Proc. IEEE SECON'17, San Diego, CA, June 2017, pp. 1–9.
[32] Z. Zhou, L. Shangguan, X. Zheng, L. Yang, Y. Liu, Design and implementation of an RFID-based customer shopping behavior mining system, IEEE/ACM Trans. Netw. 25 (4) (Aug. 2017) 2405–2418.
[33] ROS [online] Available: http://www.ros.org/. Accessed on June. 4, 2018.
[34] S. Umeyama, Least-squares estimation of transformation parameters between two point patterns, Trans. Pattern Anal. Mach. Intell. 13 (4) (Apr. 1991) 376–380.
[35] D.W. Eggert, A. Lorusso, R.B. Fisher, Estimating 3-D rigid body transformations: a comparison of four major algorithms, Mach. Vis. Appl. 9 (5/6) (Mar. 1997) 272–290.